

A Reference Governor for Plasma-Shape Control in Tokamaks

Andres Pajares, William P. Wehner, Anders S. Welander, Eugenio Schuster, and David A. Humphreys

Abstract—Tokamaks are torus-shaped devices where a high-temperature, ionized gas (i.e. a plasma) is confined by means of helical magnetic fields. The ultimate goal of tokamaks is producing net electrical energy by means of nuclear-fusion reactions within the plasma. The shape of the plasma inside the tokamak is closely related with its confinement characteristics and, therefore, with the produced fusion power. In order to achieve and maintain plasma shapes that maximize the fusion yield, feedback controllers have been successfully developed during the years. However, machine-protection and plasma-stability requirements impose hard constraints on the plasma-shape targets that can be safely achieved by a feedback controller. In this work, a reference governor is proposed to provide, in real time, plasma-shape targets that fulfill the aforementioned safety requirements. The reference governor calculates such plasma-shape targets in response to changes in the state of the closed-loop system, as well as disturbances in the plasma energy and current. The reference-governor design is based on a dynamical model of the plasma electromagnetic response. Simulation tests of the reference governor have been carried out for different plasma scenarios in the DIII-D tokamak to emulate realistic cases where safety may be compromised.

I. INTRODUCTION

Nuclear fusion is the process that powers the Sun and the stars. In a nuclear-fusion reaction, light atoms (usually hydrogen, helium, and/or its isotopes) combine to form heavier atoms while releasing high amounts of energy per mass unit. This process happens naturally in the stars because large gravitational forces make the nuclei of the atoms overcome the Coulombic force that repels them. Due to the high temperatures necessary for nuclear fusion to happen, the reactants are in plasma state (i.e. a gas where ions and electrons are dissociated, so electrical currents can flow through it). On Earth, ways of achieving nuclear fusion are being studied for energy generation purposes. So far, one of the most promising concepts is the so-called “tokamak”

This material is based upon work supported by General Atomics corporate funding, and by the U.S. Department of Energy, Office of Science, Office of Fusion Energy Sciences, using the DIII-D National Fusion Facility, a DOE Office of Science user facility, under Award(s) DE-FC02-04ER54698. A. Pajares (pajaresa@fusion.gat.com), W. Wehner, A. Welander, and D. Humphreys are with the Plasma Control and Operations Group, General Atomics, San Diego, CA 92121, USA. E. Schuster is with the Department of Mechanical Engineering and Mechanics, Lehigh University, Bethlehem, PA 18015, USA. Disclaimer: This report was prepared as an account of work sponsored by an agency of the U.S. Government. Neither the U.S. Government nor any agency thereof, nor any of their employees, makes any warranty, express or implied, or assumes any legal liability or responsibility for the accuracy, completeness, or usefulness of any information, apparatus, product, or process disclosed, or represents that its use would not infringe privately owned rights. Reference herein to any specific commercial product, process, or service by trade name, trademark, manufacturer, or otherwise does not necessarily constitute or imply its endorsement, recommendation, or favoring by the U.S. Government or any agency thereof. The views and opinions of authors expressed herein do not necessarily state or reflect those of the U.S. Government or any agency thereof.

(a Russian acronym that stands for “toroidal chamber with magnetic coils”), where a plasma is confined within a torus-shaped machine by means of helical magnetic fields. A diagram of the tokamak device is shown in Fig. 1.

The shape that the plasma achieves within the magnetic cage created by the tokamak has a high impact on the quality of the plasma confinement, as well as on the macroscopic stability of the plasma column (also referred to as magnetohydrodynamic (MHD) stability [1]). For instance, highly elongated plasmas (i.e. plasmas where the height of the poloidal cross section is significantly larger than its width, see Fig. 1) present an improved confinement [2], but also tend to move vertically in an unstable manner (i.e. the well-known vertical instability [1]). Therefore, the operation and optimization of present and future tokamak designs substantially relies on the shaping capabilities of a tokamak as well as on the stabilization of the vertical plasma motion. As a result, vertical stability and shape control is one of the problems of major interest in nuclear-fusion research. Feedback control of the vertical position and plasma shape can usually be done in present tokamaks by a set of conducting coils that surround the plasma (see Fig. 1) and exert forces on it according to Lorentz’s law [1]. A large number of vertical stability and shape controllers have been developed and are currently operating in tokamaks all around the world. Examples of such designs can be found for tokamaks such as C-mod [3], DIII-D [4], TCV [5], ASDEX-U [6], KSTAR [7], JET [8], NSTX [9], JT60-SA [10], and EAST [11], among many others. These controllers enable much of the present and future fusion-research program. In fact, as of now, shape control is one of the most mature fusion-control problems.

In addition to the maximization of the plasma confinement and MHD stability, shape control is also necessary to prevent undesired events that may risk the integrity of the tokamak device. An example of such type of events is a plasma-wall contact, i.e. the partial intrusion of the plasma into the solid first-wall of the tokamak. During a plasma-wall contact, a significant influx of impurities (usually atoms with higher atomic mass than hydrogen) is normally found which may deteriorate the plasma confinement. Moreover, damage to the machine may occur due to high heat fluxes from the plasma into the surrounding tokamak structures. Another example are vertical displacement events, i.e. the vertical motion of the plasma column due to its inherent vertical instability [1]. Such vertical motion often ends with a wall contact and/or a disruption, i.e. a sudden loss of plasma confinement that imposes high current and heat loads on the plasma facing components. The avoidance of this type of events is of the highest importance for the next generation of reactor-grade

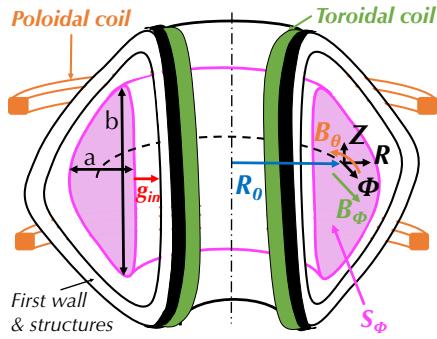


Fig. 1. Diagram of a tokamak with: a) plasma, delimited by the magenta boundary and with cross-section S_ϕ , b) first wall and surrounding structures, c) toroidal coils (shown in green) which generate the toroidal magnetic field B_ϕ along the ϕ axis, and d) poloidal coils (shown in orange) which modify the poloidal magnetic field B_θ within the R - Z plane and enable plasma shaping. The elongation is $\kappa \triangleq b/a$, where b and a are the characteristic height and length of the plasma, respectively. The inner gap g_{in} (shown in red) is the plasma-wall distance on the innermost part of the tokamak torus.

tokamaks led by ITER [12], currently under construction. Advanced control algorithms, sometimes with supervisory and exception handling capabilities, are necessary to ensure the safety of the closed-loop system (i.e. the open-loop plant composed of plasma and tokamak, plus the shape controller). Examples can be found in [13], [14], [15], [16], [17], [18].

Along this line of advanced-control research for enhanced system performance and protection, this work proposes the use of a reference governor [19] to ensure closed-loop safety for the shape-control problem in tokamaks. Safety is specified by means of limits on parameters such as, for example, plasma-wall gaps (i.e. the distance between the plasma boundary and the tokamak first wall at some points) or elongation, see Fig. 1. The reference governor calculates, in real time, plasma-shape targets that maintain the closed-loop system safe. Such targets are updated in response to changes in the system state and disturbance levels. The targets from the reference governor are provided to a feedback controller, which is in charge of regulating the plasma shape and maintaining vertical stability. The reference governor is based on a linear, time-invariant (LTI) model obtained with GSDesign [20], which models the electromagnetic response of the plasma to changes in the voltage applied to the tokamak coils as well as disturbances in the plasma current and energy. Simulations are carried out to test the performance of the overall control scheme, i.e. the combination of the reference governor and the plasma-shape feedback controller. Realistic cases, such as plasma-wall contacts and vertical-displacement events, are considered. A first case is studied for the avoidance of a plasma-wall contact in the DIII-D tokamak. A second case for the avoidance of a vertical-displacement event is emulated with a linear, time-variant (LTV) model provided by GSUpdate [20]. Therefore, in the second case, the LTV model used for the simulation is more general than the LTI model used within the reference governor. In addition, two plasma scenarios are used to test the scheme under different plasma conditions.

This paper is organized as follows. The dynamical model of the electromagnetic plasma response is given in Section II. The reference governor is presented in Section III. The sim-

ulation study is included in Section IV. Finally, conclusions and possible future work are presented in Section V.

II. DYNAMICAL MODEL OF THE PLASMA ELECTROMAGNETIC RESPONSE

A. Open-loop Dynamics

The model for the reference governor is obtained using GSDesign [20]. The model characterizes how the plasma shape and vertical position change in response to variations in the coil voltages and plasma disturbances near a given equilibrium. Such plasma equilibrium respects the MHD momentum equation [1] within the R - Z plane (see Fig. 1) in steady state as given by $\nabla p = \vec{j} \times \vec{B}$, where p is the plasma pressure, \vec{j} is the current density, and \vec{B} is the magnetic field. The model is valid around an equilibrium from a real plasma discharge in a tokamak. This particular equilibrium is denoted as “nominal equilibrium” in the rest of this paper.

The dynamical model in GSDesign is given by

$$\frac{dx}{dt} = Ax + Bu + B'w, \quad y = y_0 + Cx + D'w, \quad (1)$$

where the following model variables are defined. First, x contains the currents that flow through the magnetic coils (denoted as $I_c = [I_{c,1}, \dots, I_{c,n_c}]^T$, where n_c is the total number of magnetic coils used for control), as well as the currents that may be driven within the other conducting structures of the tokamak (denoted by $I_v = [I_{v,1}, \dots, I_{v,n_v}]^T$, where n_v is the total number of conducting structures). Therefore, $x \in \mathbb{R}^{n_c+n_v}$. Second, $u = [V_{c,1}, \dots, V_{c,n_c}]^T$ contains the voltages applied to the poloidal-field coils, $V_{c,i}$, for $i = 1, \dots, n_c$. Therefore, $u \in \mathbb{R}^{n_c}$. Third, y contains different descriptors of the plasma shape, such as the elongation and the distance between the plasma boundary and the tokamak first wall (i.e. gaps). The number of outputs is denoted by n_y , so $y \in \mathbb{R}^{n_y}$. Finally, the disturbance $w \in \mathbb{R}^3$ contains three plasma variables: total current, $I_p = \int_{S_\phi} \vec{j} \cdot d\vec{S}_\phi$ (where S_ϕ is the poloidal cross section of the plasma, shaded in magenta within Fig. 1), poloidal beta, $\beta_p = \frac{4}{I_p^2 \mu_0 R_0} \int_V p dV$ (where R_0 is the value of the radial coordinate R at the torus axis, see Fig. 1, and V is the plasma volume), and internal inductance, $l_i = \frac{1}{I_p^2 \mu_0 R_0} \int_V B_\theta^2 dV$ (where B_θ is the poloidal magnetic field). It can be noted that β_p is a proxy for the plasma thermal energy ($\beta_p \propto pV$), and l_i characterizes the spatial distribution of B_θ within the plasma. Finally, A , B , B' , C , D' , and y_0 are constant, and y_0 characterizes the model output when $x = w = 0$.

Under the steady-state conditions reached at the nominal equilibrium, the components of I_v are usually much smaller than I_c (i.e. $I_c \gg I_v \approx 0$), and $dI_v/dt \approx 0$. This allows for calculating an equilibrium value for u (denoted as \bar{u}) that maintains a given set of equilibrium coil currents, \bar{I}_c , with $d\bar{I}_c/dt = 0$. The value of \bar{u} can be obtained from (1), which can be rewritten at the nominal equilibrium as

$$B\bar{u} = -A[\bar{I}_c, \bar{0}]^T. \quad (2)$$

Because of the physics and circuit equations embedded in GSDesign, B is full rank, so (2) has a unique solution.

Nominal and deviation variables are defined as $\bar{x} \triangleq [\bar{I}_c, \bar{0}]^T$, $\bar{w} \triangleq [\bar{I}_p, \bar{l}_i, \bar{\beta}_p]^T$ (where \bar{I}_p , $\bar{\beta}_p$, and \bar{l}_i correspond to the nominal equilibrium), $\bar{y} = y_0 + C\bar{x} + D'\bar{w}$, $\tilde{I}_c \triangleq I_c - \bar{I}_c$, $\tilde{I}_v \triangleq I_v$, $\tilde{x} \triangleq x - \bar{x}$, $\tilde{u} \triangleq u - \bar{u}$, $\tilde{w} \triangleq w - \bar{w}$, and $\tilde{y} \triangleq y - \bar{y}$. Therefore, (1) is rewritten as

$$\frac{d\tilde{x}}{dt} = A\tilde{x} + B\tilde{u} + B'\tilde{w}, \quad \tilde{y} = C\tilde{x} + D'\tilde{w}. \quad (3)$$

B. Closed-loop Dynamics

For most plasma shapes of interest, the matrix A has one positive eigenvalue that corresponds to the vertical-instability growth rate, γ_z [1]. Therefore, the open-loop dynamics (3) is unstable, and feedback control is usually employed to stabilize the plasma vertical position as well as for overall shape control. In this work, a linear-quadratic-integral (LQI) controller is employed. The goal is to make the closed-loop system vertically stable, and also to make \tilde{y} track a desired target denoted by \tilde{r} . The LQI controller is obtained from [21]

$$\min_K \int_0^\infty (z^T Q z + \tilde{u}^T R \tilde{u}) dt, \quad \text{subject to} \quad (4)$$

$$\text{System dynamics (3) with } \tilde{u} = Kz \quad (5)$$

where $Q \in \mathbb{R}^{(n_c+n_v+n_y) \times (n_c+n_v+n_y)}$ and $R \in \mathbb{R}^{n_c \times n_c}$ are design matrices, $z \triangleq [\tilde{x}, \int(\tilde{r} - \tilde{y}) dt]^T$, and $K \in \mathbb{R}^{n_c \times (n_c+n_v+n_y)}$ is the controller matrix which is found by solving (4)-(5). Under feedback, (3) becomes

$$\frac{d\tilde{x}_{CL}}{dt} = A_{CL}\tilde{x}_{CL} + B_{CL}\tilde{r} + B'_{CL}\tilde{w}_{CL}, \quad (6)$$

$$\tilde{y} = C_{CL}\tilde{x}_{CL} + D'_{CL}\tilde{w}_{CL}, \quad (7)$$

where A_{CL} , B_{CL} , B'_{CL} , C_{CL} , D'_{CL} , \tilde{x}_{CL} , and \tilde{w}_{CL} are defined within Appendix I, together with the details of the derivation of the closed-loop, state-space model (6)-(7).

III. REFERENCE-GOVERNOR ALGORITHM

The reference-governor algorithm in [19] can be applied to (6)-(7) if such dynamical model fulfills the following assumptions: 1) A_{CL} is asymptotically stable, and 2) the pair (A_{CL}, C_{CL}) is observable. The first assumption is fulfilled due to the LQI controller, which ensures vertical stability under feedback (see Section II-B). For the second assumption, the open-loop system (1) provided by GSDesign is fully observable, but the closed-loop system (6)-(7) is not (see Appendix I). However, (6)-(7) has $n_c + n_v$ observable states, so it is possible to find an observable realization [22],

$$\frac{d\hat{x}}{dt} = \hat{A}\hat{x} + \hat{B}\hat{r} + \hat{B}'\hat{w}, \quad \hat{y} = \hat{C}\hat{x} + \hat{D}'\hat{w}, \quad (8)$$

where $\hat{x} \in \mathbb{R}^{n_c+n_v}$ is the observable state (which is different from \tilde{x}_{CL} in general), $\hat{y} \equiv \tilde{y}$, $\hat{r} \equiv \tilde{r}$, $\hat{w} \equiv \tilde{w}_{CL}$, and $\hat{A} \in \mathbb{R}^{(n_c+n_v) \times (n_c+n_v)}$, $\hat{B} \in \mathbb{R}^{(n_c+n_v) \times n_c}$, $\hat{B}' \in \mathbb{R}^{(n_c+n_v) \times 3}$, $\hat{C} \in \mathbb{R}^{n_y \times (n_c+n_v)}$, and $\hat{D}' \equiv D'_{CL}$ are the model matrices corresponding to the observable state-space realization.

For a generic variable denoted by q , its time derivative is discretized as $dq/dt \approx [q(t + \Delta t) - q(t)]/\Delta t$, where Δt is the discretization time-step. Therefore, (8) is discretized as

$$\hat{x}_{k+1} = A_d\hat{x}_k + B_d\hat{r}_k + B'_d\hat{w}_k, \quad (9)$$

$$\hat{y}_k = C_d\hat{x}_k + D'_d\hat{w}_k, \quad (10)$$

where $q_k \triangleq q(t = k\Delta t)$ (for $k = 0, 1, \dots, \infty$), $A_d \triangleq I + \Delta t\hat{A}$, $B_d \triangleq \Delta t\hat{B}$, $B'_d \triangleq \Delta t\hat{B}'$, $C_d \triangleq \hat{C}$, $D'_d \triangleq \hat{D}'$, and I is the identity matrix of size $n_c + n_v$.

A. Reference-Governor Synthesis and Control Law

As depicted in Fig. 2, the function of the reference governor is to substitute the desired target \hat{r} (which is potentially unsafe) with a safe target denoted by \hat{v} . To do this, the reference governor takes \hat{x} as an input, together with the set of potential disturbances \hat{w} , and the safe set where \hat{y} must lie. The design of the reference governor in this work is mostly based on the algorithm presented in [19]. Here, a less formal derivation with some additions is provided.

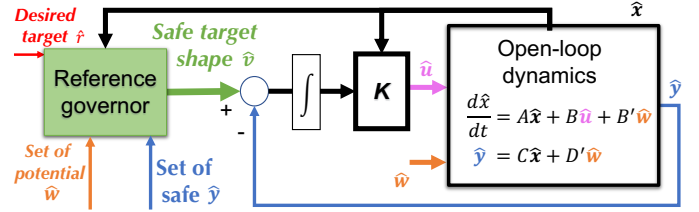


Fig. 2. Diagrams of the traditional closed-loop system for shape control (top) and with the addition of a reference governor (bottom).

At each sampling time $t = k\Delta t$, the reference governor updates \hat{v} according to the control law given by

$$\hat{v}_{k+1} = \hat{v}_k + K_{RG}(\hat{r}_k - \hat{v}_k), \quad (0 \leq K_{RG} \leq 1) \quad (11)$$

where K_{RG} is the reference-governor gain. By means of (11), the goal is to ensure that \hat{y}_k remains within the safe set, $[Y^{min}, Y^{max}]$, at all future times under feedback, i.e.

$$Y^{min} \leq \hat{y}_k \leq Y^{max}, \quad k \in \mathbb{Z}^+, \quad (12)$$

for all $W^{min} \leq w \leq W^{max}$, where $W^{min}, W^{max} \in \mathbb{R}^3$ characterize the limits of the potential disturbances experienced by the system, and $Y^{min}, Y^{max} \in \mathbb{R}^{n_y}$ characterize the boundaries of the safe output set. To rewrite (12), a “disturbance-free” version of (9) is used with $\hat{w}_k \equiv 0$, i.e.

$$x_{k+1}^* = A_d x_k^* + B_d \hat{v}_k, \quad x_0^* = \hat{x}_0, \quad (13)$$

where x_k^* is the “disturbance-free” state, and \hat{x}_0 is the initial state (which is the same for (9) and the disturbance-free case (13)). Using (10) and the definition of x^* in (13), the $k = 1$ constraint in (12) becomes

$$Y_1^{min} \leq C_d x_1^* \leq Y_1^{max}, \quad \forall \hat{w} \in [W^{min}, W^{max}], \quad (14)$$

where $Y_1^{min} \triangleq Y^{min} \sim D'_d w_1^{min}$ and $Y_1^{max} \triangleq Y^{max} \sim D'_d w_1^{max}$ are the output limits modified by the effect of \hat{w} through D'_d in (10), \sim denotes the Minkowsky subtraction [19], and w_1^{min} and w_1^{max} are found by solving two linear programs given by

$$\begin{aligned} \min_{w_1^{min}} D'_d w_1^{min}, \quad \text{subject to } W^{min} \leq w_1^{min} \leq W^{max}, \\ \max_{w_1^{max}} D'_d w_1^{max}, \quad \text{subject to } W^{min} \leq w_1^{max} \leq W^{max}. \end{aligned}$$

Similarly, all $k \geq 2$ constraints in (12) can be expressed as

$$Y_k^{min} \leq C_d x_k^* \leq Y_k^{max}, \quad (15)$$

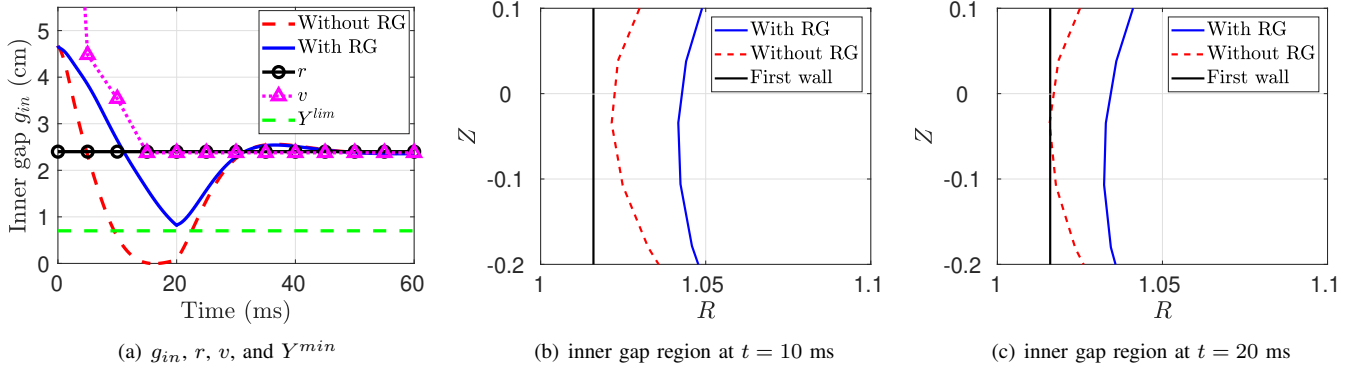


Fig. 3. Simulation for plasma-wall contact avoidance in DIII-D high- q_{min} plasma: inner gap evolution and plasma shape within inner-gap region.

where $Y_k^{min} \triangleq Y_{k-1}^{min} \sim C_d A_d^{k-2} B'_d \hat{w}_k^{min}$ and $Y_k^{max} \triangleq Y_{k-1}^{max} \sim C_d A_d^{k-2} B'_d \hat{w}_k^{max}$ are the safe output limits modified by the effect of \hat{w} through (9), and w_k^{min} and w_k^{max} are found by solving the following linear programs,

$$\begin{aligned} \max_{w_k^{min}} C_d A_d^{k-2} B'_d w_k^{min}, \quad \text{subject to } W^{min} \leq w_k^{min} \leq W^{max}, \\ \min_{w_k^{max}} C_d A_d^{k-2} B'_d w_k^{max}, \quad \text{subject to } W^{min} \leq w_k^{max} \leq W^{max}. \end{aligned}$$

The reference governor tries to maximize the gain K_{RG} defined in (11) while fulfilling (14)-(15), i.e. it tries to make the safe target \hat{v} as close as possible to the desired target \tilde{r} while keeping \hat{y} safe for all values of \hat{w} . Such task can be formulated as a linear optimization problem. By defining the sets Y_k delimited by Y_k^{min} and Y_k^{max} ($k \in \mathbb{Z}^+$), and a finite time $t^* \triangleq (k + \Delta k)\Delta t$ (where $\Delta k \in \mathbb{Z}^+$), the linear program at each sampling time $t = k\Delta t$ is given by

$$\max K_{RG}, \quad \text{subject to (11) and} \quad (16)$$

$$x_{l+1}^* = A_d x_l^* + B_d \hat{v}_{k+1}, \quad \forall l \in [k+1, k+\Delta k], \quad (17)$$

$$x_k^* = \hat{x}_k, \quad (18)$$

$$C_d x_l^* \in Y_{l-k}, \quad \forall l \in [k+1, k+\Delta k], \quad (19)$$

$$H_0 [\hat{v}_k + K_{RG} (\hat{r}_k - \hat{v}_k)] \in Y_\infty, \quad (20)$$

where $H_0 \triangleq C_d(I - A_d)^{-1}B_d$ is the static gain of (9)-(10), and Y_∞ is a set that lies in the interior of the intersection of all the sets Y_k up until t^* , i.e. $Y_\infty \subset \text{int}(\bigcap_{k=1}^{k=t^*} Y_k)$. From (17)-(20), it can be seen that the reference governor needs to sample \hat{r}_k , \hat{x}_k and \hat{v}_k (i.e. the safe target from the previous sampling time) and needs to know the limits Y^{min} , Y^{max} , W^{min} , and W^{max} which are embedded within the sets Y_k .

IV. SIMULATION STUDY

For these simulations, the DIII-D tokamak is considered. Some machine parameters of interest are $a = 0.6$ m, $R_0 = 1.7$ m, and $B_\phi \in [1.7, 2.1]$ T. Two cases are studied: the avoidance of a plasma-wall contact (Section IV-A) and the prevention of a vertical-displacement event (Section IV-B).

A. Plasma-Wall Contact Avoidance

In this section, the control scheme is tested in simulations that use the same model as in (1), i.e. both the LQI controller and the reference governor know exactly the model matrices A , B , B' , C , and D' , and the vector y_0 .

The simulation scenario of this section corresponds to DIII-D shot 172538, which belongs to the high- q_{min} scenario (a candidate for steady-state operation in ITER [23]). The plasma parameters in \bar{w} are given by $I_p = 1.05$ MA, $l_i = 0.79$, and $\beta_p = 1.59$. The output in this case is $y = g_{in}$, where g_{in} is the inner gap (see Fig. 1). An LQI controller (see Section II-B and Appendix I) is used to vertically stabilize the plasma and also regulate g_{in} . The inner-gap target is $r = 2.4$ cm, which is smaller than its nominal value of $\bar{y} = \bar{g}_{in} = 4.7$ cm. This choice for r tries to emulate an experimental situation in which it is desired to reduce g_{in} as much as possible while still having $g_{in} > 0$, which can be beneficial for certain MHD instabilities [1]. However, a perturbation $\tilde{w} \neq 0$ introduced emulating a loss of plasma confinement, so l_i is increased from its nominal value of 0.79 up to 0.97, whereas β_p decreases from 1.59 to 1.24. These changes for w occur within the first 20 ms of the simulation, and they are expected to also push the plasma toward the wall and reduce g_{in} even more, possibly making $g_{in} = 0$. Therefore, within the reference governor, a lower limit on g_{in} is imposed given by $Y^{min} = 0.7$ cm. The goal of the simulation is testing how the reference governor modifies r so that g_{in} remains within the safe limit specified by Y^{min} , and the plasma does not make contact with the wall.

Fig. 3(a) shows g_{in} without and with the reference governor, together with the targets v and r , and the limit Y^{min} . Without the reference governor, the undesired contact ($g_{in} \approx 0$) happens briefly when $t \approx [15, 20]$ ms. Later, g_{in} is driven to r . With the reference governor, the inner-gap target v is increased with respect to r when $t \approx [0, 15]$ ms. Although g_{in} does not converge toward v within such period of time, contact between the plasma and the wall is avoided. In fact, $g_{in} > Y^{min} > 0$ at all times. Before the end of the simulation, g_{in} converges toward v . Fig. 3(b) and Fig. 3(c) show zoomed-in views in the R - Z plane of the inner-gap region of the plasma at $t = 10$ ms and $t = 20$ ms. The first wall of DIII-D is also shown. Although the initial shapes in the inner-gap region are the same, the modifications to v made by the reference governor yield a higher g_{in} , and the plasma is further away from the first wall (see Fig. 3(b)). Because of this, later on, a temporary plasma-wall contact can be appreciated without the reference governor which is avoided in the case with the reference governor (see

Fig. 3(c)). Finally, at the end of the simulation, the inner gap is almost identical with and without the reference governor (see Fig. 3(a)) because $v \rightarrow r$ (i.e. $K_{RG} \rightarrow 1$).

B. Vertical-Displacement Event Avoidance

In this section, the reference governor is tested in simulations where the open-loop dynamics (see Fig. 2) is obtained with GSUpdate [20], which provides a LTV model given by

$$\frac{dx}{dt} = A(t)x + B(t)u + B(t)'w, \quad (21)$$

$$y = y_0(t) + C(t)x + D(t)'w, \quad (22)$$

where all the variables have same meaning as in Section II, but A , B , B' , C , D , and y_0 change in time. GSUpdate can accurately simulate phenomena where the plasma equilibrium varies significantly, such as vertical displacement events, and has enabled the model-based design of vertical stability and shape controllers [20]. Therefore, the LTV model (21)-(22) used in this section is more general than the LTI model (1) from Section II, which is still used for the design of the reference governor and LQI controller.

The simulation scenario corresponds to shot 184250, which has an ITER-like shape scaled to fit within the DIII-D vessel. The plasma parameters are $I_p = 0.98$ MA, $l_i = 1.31$, and $\beta_p = 0.27$. This simulation is a partial emulation of the experiment reported in [17]. The output is $y = [\kappa, \gamma_z]^T$, where κ is the elongation (see Fig. 1) and γ_z is the vertical-instability growth rate. An LQI controller (see Section II-B) is used to vertically stabilize the plasma while also primarily regulating κ but not γ_z (i.e. the terms in Q corresponding to κ are designed to be much higher than those corresponding to γ_z). The elongation target in r is ramped at a rate of 0.2 s^{-1} from its nominal value of $\bar{\kappa} = 1.75$. In addition, within the reference governor, an upper limit on γ_z of 1500 rad/s is imposed, whereas a limit for κ is not specified, i.e. $Y^{max} = [\infty, 1500 \text{ rad/s}]^T$. Because elongated plasmas are more unstable, it is expected that γ_z increases as the LQI controller ramps up κ [17]. The goal of the simulation is testing how the reference governor modifies r so that γ_z remains below Y^{max} to avoid a vertical displacement event.

Fig. 4 shows κ together with the associated components of the targets v and r (see Fig. 4(a) and Fig. 4(b)) and γ_z with its limit in Y^{max} (see Fig. 4(c)) obtained with (solid blue) and without (red dashed) the reference governor, which is abbreviated as RG in the figures of this section. The simulation is executed for $t \in [0, 0.32]$ s. Due to the relatively high variations in κ during the simulation without the reference governor, Fig. 4(a) shows κ in $t \in [0, 0.28]$ s, and Fig. 4(b) shows κ in $t \in [0.27, 0.315]$ s. Fig. 5 shows the plasma shape with and without the reference governor at different time instants, together with DIII-D's first wall. In Fig. 4(a), from $t = 0$ until $t \approx 0.21$ s, κ is ramped up both with and without the reference governor, so the plasma follows the same evolution in both cases with $r = v$ (i.e. $K_{RG} = 1$). When $t \gtrsim 0.21$ s, the reference governor identifies a potential safety violation due to the proximity of the limit Y^{max} (see Fig. 4(c)), and caps v to about 1.8. After

this, v is kept constant by the reference governor as shown in Fig. 4(a) and Fig. 4(b) ($v \neq r$, so K_{RG} goes from 1 to 0), so that $\gamma_z < Y^{max}$ (see Fig. 4(c)). Because the reference governor keeps v constant, changes to the plasma shape are minimal when $t \gtrsim 0.21$ s. On the other hand, without the reference governor, κ keeps increasing to track r , and some oscillations are found at $t \approx 0.28$ s with a partial loss of vertical control (see Fig. 4(b) and Fig. 5(a)) due to the large γ_z above Y^{max} (see Fig. 4(c)). Recovery of the plasma shape is achieved shortly after, as shown in Fig. 4(b). However, at $t \approx 0.315$ s, oscillations are found again (see Fig. 4(b) and Fig. 5(b)) where the plasma moves vertically and touches the wall with a total loss of control. Eventually, the plasma collapses to a small, almost circular shape ($\kappa \approx 1$) limited on the wall (see Fig. 5(c)) very different from the desired κ .

V. CONCLUSIONS AND FUTURE WORK

A model-based reference governor is proposed in this work to ensure tokamak-plasma safety when doing shape control. Updates to the plasma-shape target are calculated online by the reference governor, which takes into account real-time changes to the system state and disturbances. Because the reference governor is an external loop to the feedback controller, independent design of both components is possible. Successful performance is shown in simulations to prevent undesirable events such as plasma-wall contacts and vertical-displacement events. Even when the reference governor does not have perfect knowledge of the plasma dynamics (as in Section IV-B), safety is ensured as long as the modeled dynamics remains representative of the true system dynamics. This is an advantage of the model-based design. Future work may include experimental tests of the algorithm in DIII-D, as well as simulations in ITER and other reactor-grade tokamaks.

APPENDIX I

STATE-SPACE MODEL UNDER LQI CONTROL

The LQI control law (5) can be rewritten as

$$\tilde{u} = K_1 \tilde{x} + K_2 \int (\tilde{r} - \tilde{y}) dt, \quad (23)$$

where K_1 contains the first $n_c + n_w$ columns of K , and K_2 contains the last n_y columns of K , so $K = [K_1, K_2]$. Substituting (23) into the state equation of (3),

$$\frac{d\tilde{x}}{dt} = (A + BK_1)\tilde{x} + BK_2 \int \tilde{r} dt - BK_2 \int \tilde{y} dt + B'w, \quad (24)$$

and using the output equation of (3) to substitute \tilde{y} in (24),

$$\begin{aligned} \frac{d\tilde{x}}{dt} = & (A + BK_1)\tilde{x} + BK_2 \int \tilde{r} dt - BK_2 C \int \tilde{x} dt \\ & - BK_2 D' \int \tilde{w} dt + B'w. \end{aligned} \quad (25)$$

Differentiating with respect to time, (25) can be rewritten as

$$\begin{aligned} \frac{d}{dt} \begin{bmatrix} x_1 \\ x_2 \end{bmatrix} = & \begin{bmatrix} A + BK_1 & -BK_2 C \\ I & O \end{bmatrix} \begin{bmatrix} x_1 \\ x_2 \end{bmatrix} \\ & \begin{bmatrix} BK_2 \\ O \end{bmatrix} \tilde{r} + \begin{bmatrix} B' & -BK_2 D' \\ O & O \end{bmatrix} \begin{bmatrix} \frac{d\tilde{w}}{dt} \\ \tilde{w} \end{bmatrix}, \end{aligned} \quad (26)$$

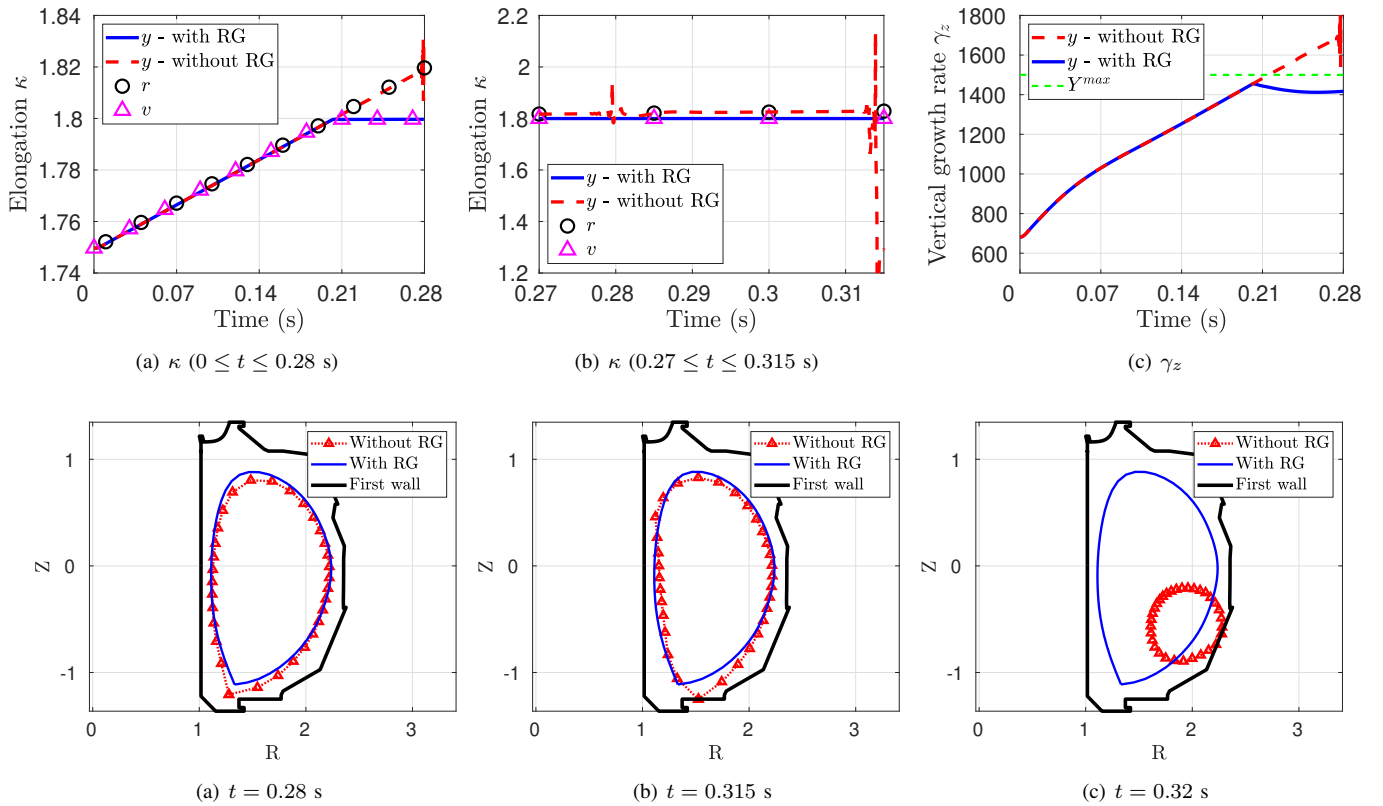


Fig. 5. Plasma shape during simulations for vertical-displacement avoidance without (red dashed) and with the reference governor (solid blue).

where $x_1 \triangleq \frac{d\tilde{x}}{dt}$ and $x_2 \triangleq \tilde{x}$. Equation (26) is rewritten as

$$\frac{d\tilde{x}_{CL}}{dt} = A_{CL}\tilde{x}_{CL} + B_{CL}\tilde{r} + B'_{CL}\tilde{w}_{CL}, \quad (27)$$

where

$$\tilde{x}_{CL} \triangleq \begin{bmatrix} \frac{d\tilde{x}}{dt} \\ \tilde{x} \end{bmatrix}, \quad A_{CL} \triangleq \begin{bmatrix} A + BK_1 & -BK_2C \\ I & O \end{bmatrix},$$

$$\tilde{w}_{CL} \triangleq \begin{bmatrix} \frac{d\tilde{w}}{dt} \\ \tilde{w} \end{bmatrix}, \quad B_{CL} \triangleq \begin{bmatrix} BK_2 \\ O \end{bmatrix}, \quad B'_{CL} \triangleq \begin{bmatrix} B' & -BK_2D' \\ O & O \end{bmatrix}.$$

Finally, (3) can be rewritten as $\tilde{y} = C_{CL}\tilde{x}_{CL} + D'_{CL}\tilde{w}_{CL}$, where $C_{CL} \triangleq [O \ C]$, and $D'_{CL} \triangleq [O \ D']$.

REFERENCES

- [1] J. Wesson, *Tokamaks*. Oxford, UK: Clarendon Press, 1984.
- [2] E. A. Lazarus *et al.*, "The role of shaping in achieving high performance in DIII-D," in *15th Int. Conf. on Plasma Physics and Controlled Nucl. Fusion*, 1994.
- [3] I. H. Hutchinson *et al.*, "Plasma shape control: a general approach and its application to Alcator C-Mod," *Fus. Technol.*, vol. 30, no. 2, 1996.
- [4] M. Walker *et al.*, "Control of Plasma Poloidal Shape and Position in the DIII-D Tokamak," in *Proc. of the 36th IEEE Conference on Decision and Control*, vol. 4, 1997, pp. 3703–3708.
- [5] H. Anand *et al.*, "A novel plasma position and shape controller for advanced configuration development on the TCV tokamak," *Nucl. Fusion*, vol. 57, no. 126026, 2017.
- [6] V. Mertens *et al.*, "Chapter 3: Plasma Control in ASDEX Upgrade," *Fusion Science and Technology*, vol. 44, no. 3, pp. 593–604, 2003.
- [7] S. Hahn *et al.*, "Design of plasma shape control system for KSTAR tokamak," in *2009 23rd IEEE/NPSS Symposium on Fusion Engineering*, 2009, pp. 1–4.
- [8] G. D. Tommasi *et al.*, "Current, position, and shape control in tokamaks," *Fusion Sci. Technol.*, vol. 59, no. 3, pp. 486–498, 2011.
- [9] D. Gates *et al.*, "Plasma shape control on the National Spherical Torus Experiment (NSTX) using real-time equilibrium reconstruction," *Nucl. Fusion*, vol. 46, pp. 17–23, 2006.
- [10] D. Corona *et al.*, "Plasma shape control assessment for JT-60SA using the CREATE tools," *Fus. Eng. Design*, vol. 146, pp. 1773–1777, 2019.
- [11] A. Mele *et al.*, "MIMO shape control at the EAST tokamak: simulations and experiments," *Fus. Eng. Design*, vol. 146, no. A, pp. 1282–1285, 2019.
- [12] D. Humphreys *et al.*, "Novel aspects of plasma control in ITER," *Phys. Plasmas*, vol. 22, p. 021806, 2015.
- [13] G. Raupp *et al.*, "Preliminary exception handling analysis for the ITER Plasma Control System," *Fus. Eng. Design*, vol. 123, pp. 541 – 545, 2017.
- [14] E. Maljaars *et al.*, "Actuator allocation for integrated control in tokamaks: architectural design and a mixed-integer programming algorithm," *Fus. Eng. Design*, vol. 122, pp. 94 – 112, 2017.
- [15] N. W. Eidietis *et al.*, "Implementing a finite-state off-normal and fault response system for disruption avoidance in tokamaks," *Nucl. Fusion*, vol. 58, p. 056023, 2018.
- [16] T. C. Blanken *et al.*, "Real-time plasma state monitoring and supervisory control on TCV," *Nucl. Fusion*, vol. 59, p. 026017, 2019.
- [17] J. L. Barr *et al.*, "Development and experimental qualification of novel disruption prevention techniques on DIII-D," *Nucl. Fusion*, vol. 61, p. 126019, 2021.
- [18] A. Pajares *et al.*, "Integrated control of individual plasma scalars with simultaneous neoclassical tearing-mode suppression," *Nucl. Fusion*, vol. 61, no. 4, 2022.
- [19] E. G. Gilbert and I. Kolmanovsky, "Fast reference governors for systems with state and control constraints and disturbance inputs," *Int. J. Robust and Nonlinear Control*, vol. 9, pp. 1117–1141, 1999.
- [20] A. S. Welander *et al.*, "Closed-loop simulation with Grad-Shafranov equilibrium evolution for plasma control system development," *Fus. Eng. Design*, vol. 146, pp. 2361–2365, 2019.
- [21] E. Sontag, *Mathematical control theory: deterministic finite dimensional systems*. Springer, 1998.
- [22] B. D. Schutter, "Minimal state-space realization in linear system theory: an overview," *J. Comput. Appl. Math.*, vol. 121, no. 1-2, pp. 331–354, 2000.
- [23] R. Buttery *et al.*, "DIII-D research to prepare for steady state advanced tokamak power plants," *J. Fusion Energy*, vol. 38, pp. 72–111, 2019.